ACS Catalysis

RESEARCH ARTICLE

pubs.acs.org/acscatalysis

Acid-Functionalized SBA-15-Type Silica Catalysts for Carbohydrate Dehydration

Anthony J. Crisci,[†] Mark H. Tucker,[∥] Ming-Yung Lee,[‡] Se Gyu Jang,[§] James A. Dumesic,*[,∥] and Susannah L. Scott*[,†,‡]

[†]Department of Chemistry & Biochemistry, [‡]Department of Chemical Engineering, and [§]Materials Research Laboratory, University of California, Santa Barbara, California 93106, United States

[∥]Department of Chemical Engineering, University of Wisconsin, Madison, Wisconsin 53706-1607, United States

Supporting Information

ABSTRACT: A bifunctional silane, 3-((3-(trimethoxysilyl)-propyl)thio)propane-1-sulfonic acid (TESAS), was designed for incorporation into SBA-15-type silica by co-condensation. To achieve mesopore ordering in the functionalized silica, the standard SBA-15 synthetic protocol was modified, resulting in well-formed hexagonal particles. In a variation, the thioether group of TESAS was oxidized by H_2O_2 to the sulfone during the synthesis of the modified SBA-15. The presence, concentration, and location of functional groups were assessed by elemental analysis, potentiometric titration, and ^{13}C and ^{29}Si CP/MAS NMR spectroscopy. Pore structure and particle morphology were observed by scanning electron microscopy (SEM), transmission electron microscopy (TEM), and powder X-ray diffraction (XRD). The materials were studied and compared in the selective dehydration of fructose to 5-hydroxymethylfurfural (HMF). Interestingly, the thioether-containing TESAS-SBA-15 shows higher activity in the dehydration of aqueous fructose, as well as higher selectivity toward HMF (71% at 84% conversion) than its sulfone derivative, possibly because of its more hydrophobic nature.

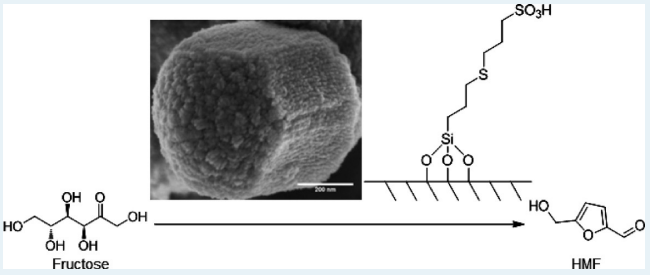

KEYWORDS: SBA-15, particle morphology, solid-state NMR, solid acid catalyst, fructose dehydration, 5-hydroxymethylfurfural

INTRODUCTION

Mesoporous ordered silicas, MOS (e.g., SBA-15), have attracted significant interest in fields ranging from biosensors, imaging, and drug delivery, to separations and catalysis.[1−6] Their reactivity depends on the nature and extent of surface functionalization, pore structure, and pore dimensions.[7−10] In a MOS synthesized for catalytic applications, it can be challenging to achieve a high loading of active sites while maintaining structural order.[11] Typically, the functional groups are incorporated by addition of an organosilane during the silica synthesis (via co-condensation), or by a postsynthetic reaction of the organosilane with surface silanols (grafting).[12] Co-condensed organosilicas possess functional groups connected to the silica support by two or three siloxane bonds, while grafted sites are typically bound by only one or two siloxane bonds.[13,14] As a result, the attachment of the functional groups in co-condensed silicas tends to be more hydrothermally stable than those of grafted sites. Although a handful of complex organosilanes have been incorporated into MOS by co-condensation,[15−19] simple derivatives of short-alkyl chains such as (3-aminopropyl)trimethoxysilane, APTMS, or (3-mercaptopropyl)trimethoxysilane, MPTMS, are usually employed.

It is possible to obtain more diversity in the functionalization of co-condensed MOS by postsynthetic derivatization.[18−22] For example, aminopropyl-functionalized SBA-15 has been further derivatized to produce anchored, melamine-based dendrimers.[23] However, it is important that the postsynthetic reactions do not disrupt the host framework or compromise the loading of functional groups. Previously, we described the synthesis of a supported bifunctional acid catalyst for the selective conversion of carbohydrates via postsynthetic derivatization of a co-condensed organosilica.[24] In that work, thiopropyl-modified SBA-15 was deprotonated with NaH, then exposed to 1,3-propanesultone to yield a material containing both thioether and sulfonic acid groups. The former was intended, upon oxidation, to promote fructose isomerization to the desired β-fructofuranose tautomer (replacing the dimethylsulfoxide (DMSO) used for this purpose in homogeneous catalysis),[25−27] while the latter catalyzes fructose dehydration to 5-hydroxymethylfurfural (HMF). Despite being significantly more stable than a similarly functionalized nonporous silica prepared entirely by grafting, the co-condensed material suffered loss of its mesopore ordering and most of its functional groups during the secondary derivatization step. The integrity of the strongly anchored co-condensed sites was compromised by silica

Special Issue: Victor S. Y. Lin Memorial Issue

Received: March 2, 2011
Revised: April 22, 2011
Published: May 05, 2011

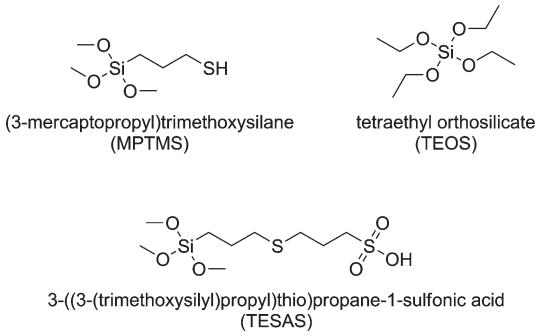

Figure 1. Structures of the various silanes used to synthesize TESAS-SBA-15, SSA-SBA-15, and pSO_3H-SBA-15.

restructuring, likely because of siloxane cleavage that occurred under the basic conditions required for thiol deprotonation.

To eliminate the need for secondary derivatization, a new silane was synthesized. Shown in Figure 1, TESAS is more complex than many organosilanes previously used in co-condensations for pore surface functionalization. In general, the weak interactions between simple organosilanes and the templating agent have little effect on pore ordering or particle morphology. However, several modifications to the standard SBA-15 synthesis protocol were required to obtain a MOS containing a significant amount of incorporated TESAS. In particular, interactions between the complex organosilane and the templating agent must be minimized by slow addition of TESAS, and by the timed addition of NaCl.

SBA-15-type materials have been obtained with a variety of particle morphologies,[28,29] which may influence their catalytic properties.[30] For example, longer retention of a substrate inside the pore channels may alter product selectivity. Morphological control can often be achieved by the addition of cosolvents or salts during synthesis.[31−33] However, there are few reports describing induced particle uniformity in functionalized SBA-type silicas synthesized by co-condensation.[34] Here, we show that it is possible to obtain well-proportioned, hexagonally shaped particles in this family of catalytically important materials.

The reaction network for fructose dehydration, Scheme 1, shows that HMF production occurs in tandem with various side-reactions. When the solvent is water, the major byproducts are soluble oligomers and insoluble humins, as well as formic and levulinic acids formed by rehydration (depending on the pH).[35] The use of an organic extracting phase suppresses these side-reactions, leading to higher HMF yields.[27] Salts (e.g., NaCl) promote partitioning of HMF into the organic phase,[36] however, their use in this study was precluded because they undergo ion-exchange with the supported Brønsted acids. HMF has also been produced in high yields with DMSO[35] or ionic liquids as solvents,[37,38] although their use increases the complexity of product isolation. In this work, a biphasic system consisting of an aqueous phase containing 30 wt % fructose and an extracting phase composed of methyl isobutyl ketone (MIBK) and 2-butanol in a 7:3 ratio was used to compare the activity and selectivity of the newly synthesized solid acid catalysts to commercially available catalysts.

Scheme 1. Reaction Network for the Dehydration of Fructose to HMF

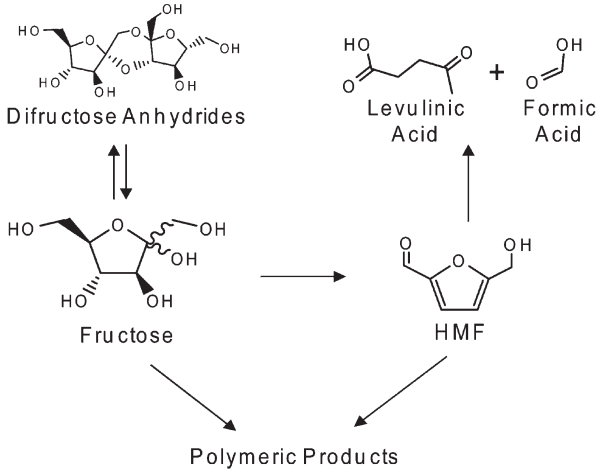

EXPERIMENTAL SECTION

Reagents and Materials. Tetraethyl orthosilicate (TEOS, > 98%), tetramethyl orthosilicate (TMOS, ≥99%), (3-mercaptopropyl)trimethoxysilane (MPTMS, 95%), sodium hydride (60% dispersion in mineral oil), 1,3-propanesultone (≥99%), ethyl acetate (ACS reagent grade), fructose (≥99%) and 2-butanol (ReagentPlus, ≥99%) were purchased from Aldrich and used as-received. Pluronic P123 was obtained from BASF. Hexanes (ACS reagent grade), NaCl, methyl iso-butyl ketone (MIBK, Certified ACS), and HCl (12 M) were purchased from Fisher Scientific. Ethanol (200 proof, Gold Shield) was used as-received. Tetrahydrofuran (THF) and diethyl ether (Aldrich) were purified by passage through two neutral Al_2O_3 columns.

All synthesized silica powders were dried under vacuum (0.1 mTorr) at 150 °C unless otherwise noted, and were stored in an argon-filled glovebox to prevent readsorption of atmospheric moisture. A 4-(ethylthio)benzenesulfonic acid-functionalized amorphous silica (Si-SPhSA, Strem), manufactured by Phosphonics, was crushed into a powder before use. Amberlyst 70, a phenylsulfonic acid-derivatized polystyrene resin (2.55 mmol H^+ g^{-1}), was obtained from The DOW Chemical Company, and was washed with Milli-Q water, dried overnight at 120 °C, and crushed before use.

Characterization. Solution-state NMR spectra were recorded on a Bruker SPX200 SB spectrometer operating at 4.7 T. Solid-state NMR spectra were recorded on a Bruker DSX500 WB spectrometer operating at 12.0 T, with frequencies of 125 and 99 MHz for ^{13}C and ^{29}Si, respectively. Samples were packed under an argon atmosphere into 4-mm zirconia rotors (Bruker). ^{29}Si cross-polarization/magic angle spinning (CP/MAS) spectra were obtained using a 90° pulse length of 2.5 μs, a contact time of 5 ms, and high power proton decoupling during detection. Typically, 25,000 scans were acquired at a spinning rate of 10 kHz. Chemical shifts were referenced to tetrakis-(trimethylsilyl)silane. ^{13}C CP/MAS spectra were obtained using a 90° pulse length of 2.4 μs, a contact time of 2 ms, and high power proton decoupling during detection. Typically, 25,000 scans were acquired at a spinning rate of 10 kHz. Chemical shifts were referenced to adamantane.

Powder X-ray diffraction (XRD) patterns were collected from 0.6 to 4° [2θ], using a Panalytical MRD PRO diffractometer with Cu K_α radiation (0.02° resolution). N_2 adsorption/desorption measurements were performed on a Micromeritics Tristar 3000 Porosimeter. Scanning electron microscopy (SEM) and transmission electron microscopy (TEM) images were acquired using a Hitachi S-4800 microscope and a FEI G^2 T20 microscope, respectively. Elemental analysis was performed by Columbia Analytical (Tuscon, AZ). In addition to elemental analysis, supported acid sites were quantified by potentiometric titration (Gran method).[39,40] Each catalyst (50 mg) was suspended in an aqueous NaCl solution (20 mL, 86 mM). The mixture was stirred for 1 h before being

titrated with NaOH (5 mM). A Beckman-Coulter pHi 510 meter was employed to record the pH during titrations.

XPS spectra were acquired using a Kratos Axis Ultra spectrometer, equipped with a monochromatic Al K_α source ($h\nu$ = 1486.6 eV), operated at 225 W (15 mA, 15 kV) and a base pressure of 1×10^{-9} Torr. Samples were degassed overnight at 1×10^{-8} Torr prior to analysis. Photoelectrons were counted with an 8-channel hemispherical detector. Photoelectron pass energies were set at 160 eV for survey spectra and 40 eV for high resolution spectra. Survey spectra are the average of two sweeps from 600 to −4 eV, with a 0.5 eV step size and a 100 ms dwell time at each step. High-resolution S 2p spectra are the average of five sweeps, with a 0.1 eV step size and an 800 ms dwell time. Spectra were processed and deconvoluted using Casa XPS version 2.3.14. A background subtraction was performed using the Shirley method. Binding energies were calibrated to extrinsic/adventitious carbon at 284.8 eV. The Marquardt root-mean-squares method was used to fit components in the high-resolution spectra.

Synthesis of Sodium 3-((3-(Trimethoxysilyl)propyl)thio)-propane-1-sulfonate (NaTESAS). To a 100 mL round-bottom flask containing NaH (0.864 g, 21.5 mmol), dry THF (30 mL) was added under flowing N_2. After cooling to −78 °C, MPTMS (4.00 mL, 21.5 mmol) was added over 15 min, and the mixture was stirred for 1 h. 1,3-Propanesultone (1.88 mL, 21.5 mmol) was added and stirring was continued for 2 h, while warming slowly to room temperature. The sodium salt of the sulfonate was recovered as white crystals using a rotary evaporator (0.1 mTorr). The solid was dissolved in about 15 mL of THF and precipitated with 30−40 mL of hexanes, collected by vacuum filtration and washed with 40 mL of hexanes. This procedure was repeated twice more, then the solid $(CH_3O)_3Si(CH_2)_3S(CH_2)_3SO_3Na$ was dried at room temperature under vacuum (0.1 mTorr) overnight. ^{1}H NMR (200 MHz, $CDCl_3$): δ 3.59 (*s*, 9H), 3.01 (*t*, 2H), 2.65 (*m*, 4H), 2.02 (*q*, 2H), 1.70 (*q*, 2H) 0.902 (*t*, 2H). ^{13}C CP/MAS NMR: δ 10 ($SiCH_2$), 24 ($CH_2CH_2SCH_2CH_2$), 31 ($Si(CH_2)_2CH_2SCH_2$), 35 ($SiCH_2)_3SCH_2$), 51 (CH_2SO_3H; $SiOCH_3$).

Synthesis of 3-(Propylthio)propane-1-sulfonic Acid-Functionalized Silica (TESAS-Silica). Pluronic P123 (6.00 g) was dissolved with stirring in 1.6 M aqueous HCl (220 mL) and heated to 35 °C in a 250 mL HDPE bottle (Nalgene).[11,41,42] TEOS (12.5 mL, 56.0 mmol) was added, followed 45 min later by solid NaTESAS (2.1 g, 6 mmol). After 24 h, the temperature was increased to 100 °C for a further 24 h. During this time, a gel formed, as well as a white powder. Both were added to a vacuum filter funnel. When distilled water was added to the funnel, the gel dissolved. The white powder was washed further with water, then the surfactant was removed by refluxing 1.00 g of solid in 500 mL of slightly acidified ethanol for 12 h. The solid was recovered by vacuum filtration and washed with 200 mL of ethanol. This extraction process was performed twice more on the powder. After the final extraction, the solid was dried at room temperature in air overnight, then at 100 °C under vacuum (0.1 mTorr) for 12 h. ^{13}C CP/MAS NMR: δ 12 ($SiCH_2$), 16 ($SiOCH_2CH_3$), 24 ($CH_2CH_2SCH_2CH_2$), 31 ($Si(CH_2)_2CH_2SCH_2$), 34 ($SiCH_2)_3SCH_2$), 51 (CH_2SO_3H), 60 ($SiOCH_2CH_3$), 70 (P123). ^{29}Si CP/MAS NMR: δ −57 (T^2), −66 (T^3), −100 (Q^3), −110 (Q^4). C: 9.35% S: 3.9%, 5.0% (results of two independent analyses).

Synthesis of 3-(Propylthio)propane-1-sulfonic Acid-Functionalized SBA-15 (TESAS-SBA-15). Pluronic P123 (2.00 g) was dissolved with stirring in 1.6 M aqueous HCl (69 mL) and heated to 35 °C in a 250 mL HDPE bottle (Nalgene).[11,41,42] TEOS (4.13 mL, 18.5 mmol) was added to the surfactant solution. After 30 min, 425 mg NaCl (7.33 mmol) was added to the reaction mixture, to produce a 0.10 M solution. After 1 h, 700 mg of solid NaTESAS (2.06 mmol) was added in 44 mg increments every 15 min for 4 h. Twenty hours later, the reaction mixture was divided equally among three Parr bombs (30 mL) fitted with Teflon liners. Each was heated at 100 °C for 24 h. The resulting suspensions were filtered, washed with water, and air-dried. The surfactant was removed by refluxing 1.30 g of TESAS-SBA-15 in 500 mL of slightly acidified ethanol for 15 h.

The solid was recovered by vacuum filtration and washed with 200 mL of ethanol. The extraction process was performed once more on the filtrate. The resulting solid was washed with water and suspended in 2 M HCl (100 mL). After 3 h, the solid was collected and washed with water until the pH of the water was neutral. The solid was dried at 60 °C in air overnight, then at 150 °C under vacuum (0.1 mTorr) for 12 h. ^{13}C CP/MAS NMR: δ 12 ($SiCH_2$), 24 ($CH_2CH_2SCH_2CH_2$), 31 ($Si(CH_2)_2CH_2SCH_2$), 34 ($SiCH_2)_3SCH_2$), 51 (CH_2SO_3H), 70 (P123). ^{29}Si CP/MAS NMR: δ −57 (T^2), −66 (T^3), −100 (Q^3), −110 (Q^4). C: 10.69%, S: 6.28%, Si: 27.71%.

Synthesis of 3-(Propylsulfonyl)propane-1-sulfonic Acid-Functionalized SBA-15 (SSA-SBA-15). The same synthesis conditions used for TESAS-SBA-15 were employed, with a small modification. After complete addition of NaTESAS, 4 equiv of H_2O_2 (30 wt % in water; 446 μL, 8.24 mmol) was added to the reaction mixture to obtain silica functionalized with $[-(CH_2)_3SO_2(CH_2)_3SO_3H]$ groups. ^{13}C CP/MAS NMR: δ 10 ($SiCH_2$), 16 ($CH_2CH_2(SO_2)CH_2CH_2$), 51 (CH_2SO_3H; $CH_2(SO_2)CH_2$), 70 (P123). ^{29}Si CP/MAS NMR: δ −57 (T^2), −66 (T^3), −100 (Q^3), −110 (Q^4). C: 7.36%, S: 3.62%, Si: 25.99%.

Synthesis of Propylsulfonic Acid-Functionalized SBA-15 (pSO_3H-SBA-15). The synthesis of pSO_3H-SBA-15 was achieved following the procedure used to prepare SSA-SBA-15, with two exceptions. First, 424 μL of MPTMS (2.06 mmol) was used instead of TESAS. It was added 1 h after the addition of TEOS, in 106 μL increments every 15 min for 1 h. Second, after complete addition of MPTMS, 6 equiv of H_2O_2 (30 wt % in water; 669 μL, 12.36 mmol) was added to the reaction mixture. ^{13}C CP/MAS NMR: δ 9 ($SiCH_2$), 17 ($CH_2CH_2SO_3H$), 51 (CH_2SO_3H;), 70 (P123). ^{29}Si CP/MAS NMR: δ −57 (T^2), −66 (T^3), −100 (Q^3), −110 (Q^4). C: 5.25%, S: 3.18%, Si: 28.69%.

Catalytic Dehydration of Fructose. To a series of thick-walled glass reactors (10 mL, Alltech), 1.5 g of an aqueous layer consisting of 30 wt % fructose in deionized water and 3.0 g of an organic layer consisting of 7:3 (w:w) MIBK:2-butanol were added with the desired amount of catalyst and a triangular magnetic stirring bar. Commercial catalysts were crushed prior to use, while the SBA-15-type silica powders were used as-is. The reactors were sealed using Teflon liners (Alltech) inserted into plastic caps. During the reaction, they were heated in a 16-well oil-filled aluminum block maintained at 130 °C and stirred at 1000 rpm. After reaction, they were cooled in a slurry of dry ice and ethylene glycol. For rate measurements, 50 mg of catalyst was used. For each catalyst, multiple experiments were performed using different total reaction times. The amount of HMF produced was plotted versus time, and the rate (as turnover frequency, TOF) was taken to be the slope of the best fit line forced through the origin, divided by the number of acid sites (determined by titration). For selectivity measurements, the amount of catalyst added was adjusted to achieve 64 μmol of H^+ in each reactor. The total reaction times were varied to obtain approximately 80% fructose conversion in each run.

After reaction, products in the aqueous and organic layers were analyzed using a Waters e2695 HPLC system. Fructose and HMF were analyzed using an Aminex HPX-87P column (Biorad) held at 85 °C, with Milli-Q water as the mobile phase at a flow rate of 0.6 mL min^{-1}. Fructose concentration was monitored using a Waters 2414 refractive index detector, while HMF concentration was determined using a Waters 2998 photodiode array detector at 320 nm. Fructose conversion was calculated as moles of fructose reacted per mole of fructose fed. HMF selectivity was calculated as moles of HMF produced per mole of fructose reacted. Levulinic acid was analyzed by HPLC using an Aminex HPX-87H column (Biorad) held at 80 °C, with 5 mM H_2SO_4 as the mobile phase and a Waters 2414 refractive index detector.

Other soluble byproducts were analyzed by LC/MS, using an Agilent 1200 series HPLC system connected to an Agilent 6320 ion trap MS

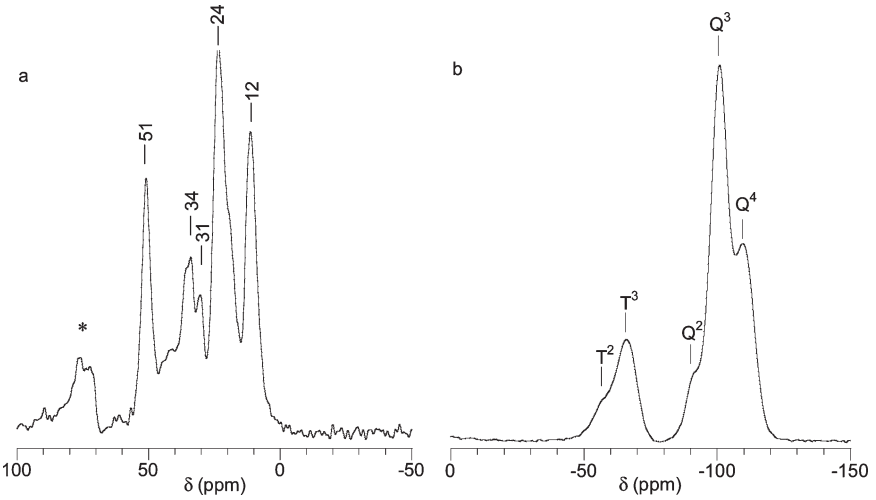

Figure 2. Solid-state NMR of TESAS-SBA-15: (a) ^{13}C CP/MAS; and (b) ^{29}Si CP/MAS spectra. Spinning rate 10 kHz. * indicates surfactant signals.

system with an atmospheric pressure chemical ionization (APCI) source in the positive mode (capillary voltage, −1 kV; corona current, 3 μA; vaporization temperature, 350 °C). A Zorbax Eclipse XDB-C18 column (4.6 × 150 mm, 5 μm; Agilent) was used at 30 °C and a flow rate of 0.5 mL min^{-1}. The mobile phases were 0.02 M $NH_4O_2CCH_3$ (Aldrich) in Milli-Q water (A) and LC/MS-grade methanol (B, Aldrich). A solvent gradient was used starting with 95:5 A:B, changing to 20:80 A:B over 10 min, then holding at 20:80 A:B.

RESULTS

Synthesis of the New Organosilane, TESAS. The sodium salt of TESAS (Figure 1) was synthesized by deprotonation of MPTMS with NaH, and the resulting thiolate was used to effect the ring-opening of 1,3-propanesultone. The ^{13}C CP/MAS NMR spectrum of NaTESAS is shown in Supporting Information, Figure S1. Signals at 31 and 35 ppm represent the two methylenes of the thioether (CH_2SCH_2). The peak at 51 ppm represents both CH_2SO_3H and $SiOCH_3$ signals. The $SiCH_2$ signal appears at 10 ppm. Signals for the methylene groups one carbon removed from either Si or the sulfonate overlap, resulting in the peak at 24 ppm and its shoulder at about 25 ppm.

Synthesis of TESAS-SBA-15. When TESAS was present during the standard hydrothermal protocol for synthesizing organofunctionalized SBA-15, involving a single addition of NaTESAS 45 min after the hydrolysis of TEOS had been initiated, both a polysiloxane gel and a white powder were recovered from the reactor. The ^{13}C and ^{29}Si CP/MAS NMR spectra of the powder showed the expected peaks for incorporated TESAS, Supporting Information, Figure S2; however, no reflections were observed by powder XRD, indicating that the pore structure of this silica is not ordered. The acid loading, assessed by potentiometric titration, was not uniform: it ranged from 0.35 to 0.75 mmol g^{-1} for different aliquots of a single batch. Similarly, the measured sulfur content was irreproducible. When TEOS and TESAS were instead added simultaneously during silica synthesis, a cloudy solution formed instead of the expected milky-white suspension of SBA-15. This procedure yielded only a gel during hydrothermal treatment at 100 °C.

TESAS-SBA-15 with a high loading of the organosilane was successfully prepared with two modifications to the synthetic procedure. Typically, NaCl is present from the start, and the organosilane is added quickly, 45 min after TEOS hydrolysis began. Instead, NaCl was added 30 min *after* TEOS hydrolysis was initiated, and the slow addition (over 4 h) of NaTESAS started 30 min later. When this mixture was subjected to hydrothermal conditions, a white powder precipitated. Its ^{13}C CP/MAS spectrum (Figure 2a) confirms the incorporation of TESAS functional groups. Signals for the methylenes adjacent to the thioether (CH_2SCH_2) are present at 31 and 34 ppm, while the signals for $CH_2CH_2SCH_2CH_2$ appear at 24 ppm. The $SiCH_2$ signal shifts from 10 ppm (NaTESAS) to 12 ppm in the co-condensed material, because of replacement of some of the methoxy groups by siloxane bonds. The relative intensity of the peak at 51 ppm is lower compared to the spectrum of NaTESAS itself. It represents both CH_2SO_3H and residual uncondensed $SiOCH_3$ groups. Signals due to template remaining after ethanol extraction are visible as a cluster of peaks at 75 ppm. Signals for $SiOCH_2CH_3$ (60, 16 ppm), expected to form during the ethanol extraction, were eliminated by washing the silica with aqueous HCl. According to the elemental analysis (C, S), residual template represents approximately 5.5 wt % in TESAS-SBA-15.

The ^{29}Si CP-MAS spectrum is typical of an organofunctionalized silica, Figure 2b. The peaks at −110, −100, and −90 ppm are attributed to the Q^4, Q^3, and Q^2 sites, respectively, of the silica framework. Organosilanes bound by two or three siloxane bonds to the silica framework (T^2 and T^3 sites) are observed at −57 and −66 ppm, respectively. The more stable T^3 sites clearly represent the majority of incorporated TESAS. The organosilane content of the ordered mesoporous silica was determined independently by both elemental analysis and potentiometric titration, Table 1. From the S/Si ratio, we deduce that the TESAS loading is 1.25 mmol g^{-1}. However, the TESAS loading inferred by titration of the strong acid sites is only 0.45 mmol g^{-1}, suggesting that a large fraction of the incorporated organosilanes is inaccessible.

In the XPS of TESAS-SBA-15, two major signals with nearly equal intensities are observed in the S 2p region, at approximately 169 and 163 eV, Figure 3a. On the basis of their binding energies, we assign them to the sulfonic acid and thioether groups, respectively, of incorporated TESAS.[43−45] In addition, a minor component at 166 eV is attributed to a sulfoxide,[43] presumably formed by partial oxidation of the thioether during hydrothermal

dx.doi.org/10.1021/cs2001237 |*ACS Catal.* 2011, 1, 719–728

Table 1. Chemical Analysis of Acidic SBA-15-Type Silicas

material	functional group	loading (mmol g^{-1}) calcd[a]	measured[b]	accessible[c]
pSO_3H-SBA-15	$-(CH_2)_3SO_3H$	1.39	1.35	1.10
TESAS-SBA-15	$-(CH_2)_3S(CH_2)_3SO_3H$	1.25	1.25	0.45
SSA-SBA-15	$-(CH_2)_3SO_2(CH_2)_3SO_3H$	1.20	0.82	0.79

[a] Expected loading for complete incorporationof organosilane. [b] Calculated from S/Si ratio obtainedby elemental analysis. [c] Measured by potentiometric titration.

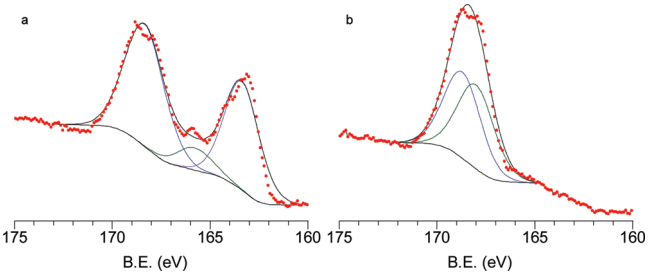

Figure 3. High resolution XPS in the S 2p region, with component deconvolutions, for (a) TESAS-SBA-15; and (b) SSA-SBA-15.

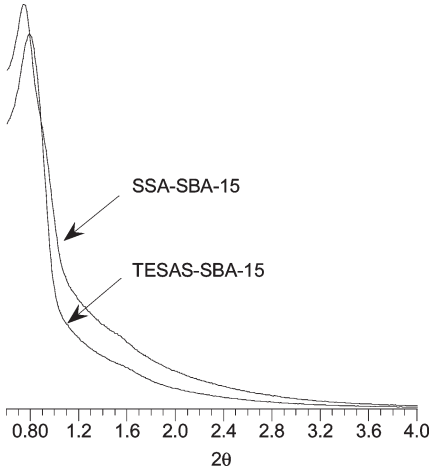

Figure 4. Low-angle XRD patterns for TESAS-SBA-15 and SSA-SBA-15.

synthesis. The ratio of the sulfonic acid signal to the thioether/sulfoxide signals is 0.98.

The powder XRD pattern is typical of an ordered mesoporous material, Figure 4, with a d_{100} reflection at $2\theta = 0.80°$. Higher-order reflections (d_{110} and d_{210}) were not observed, however, there is a weak, broad reflection at about 1.6° characteristic of organofunctionalized SBA-15.[46] N_2 sorption yielded a type IV isotherm indicating a mesoporous material, Figure 5a. The surface area and pore diameter of the TESAS-SBA-15 are 449 $m^2\ g^{-1}$ and 4.7 nm, respectively, Table 2. The 2-D hexagonal pattern of the mesopores is clearly evident in the TEM images, Figure 6a. In addition, the SEM images reveal that the particles themselves are hexagonally shaped, Figure 7.

The synthesis of TESAS-SBA-15 was also attempted using tetramethyl orthosilicate (TMOS) as the silica source. The hydrolysis rates of TESAS and TMOS are expected to be more closely matched, compared to TESAS/TEOS.[47] An ordered SBA-15-type silica was obtained when TMOS and NaTESAS were added simultaneously to an acidic solution of the templating agent at 45 °C, as judged by powder XRD. However, the amount of accessible TESAS, measured by potentiometric titration, was only 0.15 mmol g^{-1}. Consequently, this synthesis was not explored further.

Synthesis of SSA-SBA-15. To prepare the MOS containing the sulfone, an additional step was used in the procedure described above for the synthesis of TESAS-SBA-15. After complete addition of TESAS, 3 equiv of aqueous H_2O_2 was added to the reaction mixture. Following template extraction, a white powder was recovered. According to the elemental analysis (C, S), the surfactant comprises 5.1 wt % of SSA-SBA-15.

The ^{13}C CP/MAS spectrum (Figure 8a) shows that thioether oxidation was successful. In particular, the signals associated with methylenes adjacent to the thioether (CH_2SCH_2, 34 and 31 ppm) are completely absent. Upon oxidation, these signals shift to about 50 ppm, while the signals for $CH_2CH_2SCH_2CH_2$ shift from about 24 to 16 ppm. The peak at 10 ppm is attributed to $SiCH_2$, and the broad peak at 75 ppm is assigned to residual Pluronic P123. Oxidation of thioethers by H_2O_2 tends to be unselective,[48] and it is not possible to discern by ^{13}C NMR whether the product contains a sulfoxide, a sulfone, or a mixture of both. However, XPS confirms that the thioether is completely oxidized to the sulfone. In the S 2p region, no peaks associated with the thioether (163 eV) or the sulfoxide (166 ev) are present, Figure 3b. Deconvolution of the signal revealed two components present in equal amounts. Their binding energies, at 169 and 168 eV, are consistent with assignment to sulfonic acid and sulfone, respectively.[44] The ^{29}Si CP-MAS spectrum, Figure 8b, is very similar to that of TESAS-SBA-15, although the shoulder representing the minor T^2 sites is even less intense relative to the peak for the major T^3 sites.

By potentiometric titration, the number of strong acid sites present in SSA-SBA-15 is 0.79 mmol g^{-1}, Table 1. The SSA loading deduced from the elemental analysis (S/Si) is very similar, 0.82 mmol g^{-1}, demonstrating that essentially all of the SSA groups are directed toward the mesopores and therefore accessible. N_2 sorption produced a type IV isotherm (Figure 5b), with a surface area and pore diameter in the range for SBA-15 materials, Table 2. Mesopore ordering was detected by powder XRD, with a sharp reflection at $2\theta = 0.75°$ and a weak, broad reflection at about 1.6°, Figure 4. The 2-D hexagonal pattern of the mesopores was observed by TEM, Figure 9. SEM images of SSA-SBA-15 show hexagonal particles similar to those found for TESAS-SBA-15, Figure 10.

Activity and Selectivity in Fructose Dehydration. The reaction was studied in a batch reactor containing a biphasic mixture consisting of an aqueous phase containing 30 wt %

dx.doi.org/10.1021/cs2001237 |ACS Catal. 2011, 1, 719–728

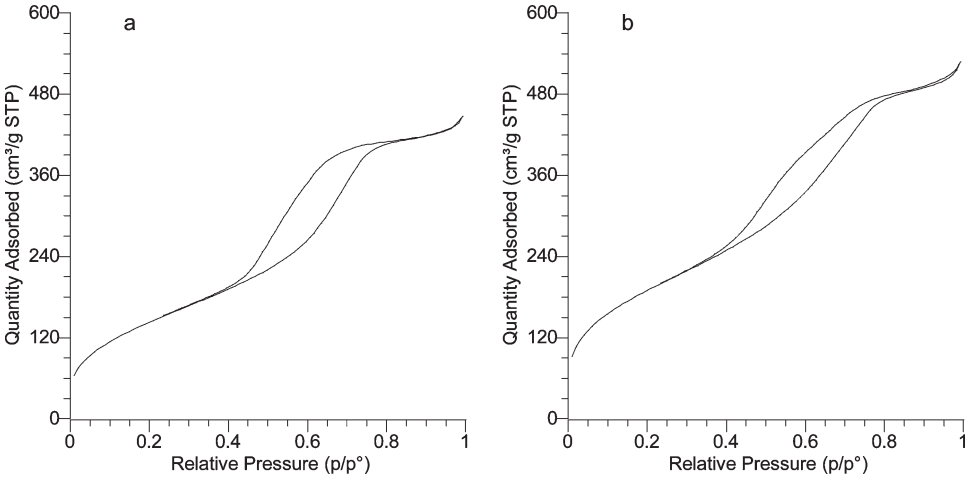

Figure 5. N_2 adsorption/desorption isotherms for (a) TESAS-SBA-15; and (b) SSA-SBA-15.

Table 2. Physical Properties of Functionalized SBA-15-Type Silicas

material	surface area,[a] $m^2\ g^{-1}$	pore size,[b] nm	pore volume,[b] $cm^3\ g^{-1}$
pSO_3H-SBA-15	640	4.5	0.90
TESAS-SBA-15	449	4.7	0.72
SSA-SBA-15	585	4.7	0.86

[a] Calculated by Brunauer–Emmett–Teller (BET) method. [b] Calculated by Barrett–Joyner–Halenda (BJH) method.

fructose and an organic extracting phase (7:3 MIBK:2-butanol) at 130 °C. Two commercial solid acid catalysts, Amberlyst 70 and Phosphonics Si-SPhSA, and one simple organofunctionalized catalyst, pSO_3H-SBA-15 (containing co-condensed propylsulfonic acid groups), were used as benchmarks. For each catalyst, the rate of HMF production is constant up to about 70% conversion, Supporting Information, Figure S8. The results are summarized in Table 3. The Weisz–Prater number is very small ($\leq 3 \times 10^{-5}$) for the silica-based catalysts, indicating that the turnover frequencies are not affected by diffusion limitations (see Supporting Information). TOF values are fairly similar for all the silica-based catalysts, although TESAS-SBA-15 and Phosphonics Si-SPhSA show the highest activities. Interestingly, while Amberlyst 70 gives the highest rate per unit mass of catalyst, it also has the highest acid loading, and consequently the lowest TOF.

To assess selectivity for HMF, the catalyst mass was adjusted to obtain the same acid concentration in each batch reaction. The reaction times were allowed to vary to reach approximately the same conversion over each catalyst. Table 4 shows that under these conditions TESAS-SBA-15 has the highest selectivity for HMF, 71%. Phosphonics Si-SPhSA, SSA-SBA-15, and pSO_3H-SBA-15 have slightly lower selectivities, while Amberlyst 70 shows the poorest selectivity for HMF, 60%. Levulinic acid was detected in both the aqueous and the organic phases. Several other side-products were detected in the aqueous phase by LC/MS (see Supporting Information). Their molecular weights suggest that they are isomers of difructose anhydrides (DFAs). In the organic phase, a dimer of HMF and addition products of HMF with MIBK and 2-butanol appear to be present. Finally, insoluble brown products, presumably humins, were observed adhering to the reactor walls and in the catalyst.

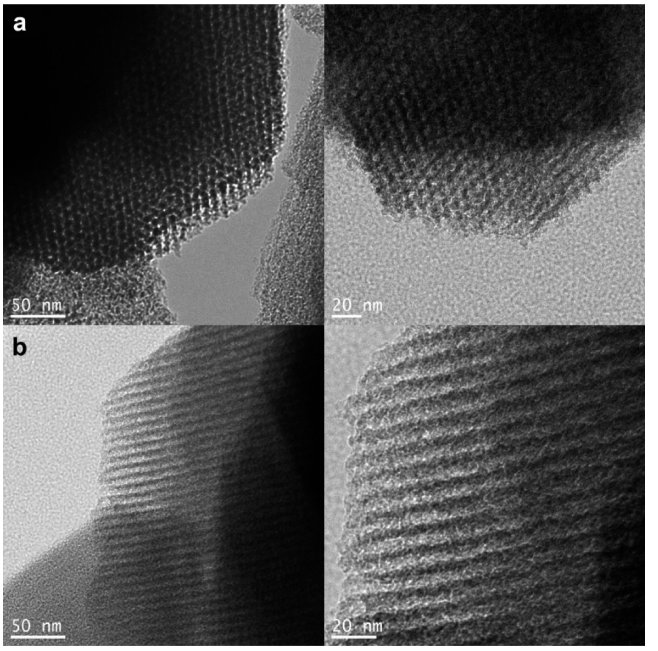

Figure 6. TEM images of TESAS-SBA-15, showing (a) the hexagonally ordered mesopores; and (b) the parallel pore channels.

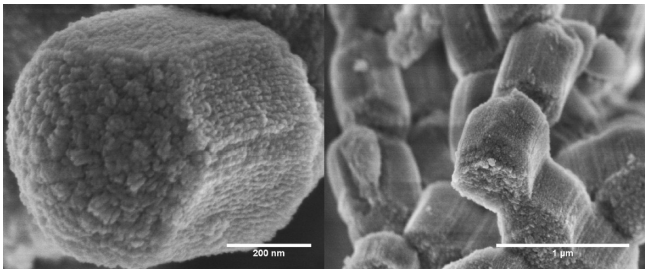

Figure 7. SEM images of TESAS-SBA-15.

DISCUSSION

Synthesis of Ordered Organofunctionalized Silicas. To suppress pore restructuring and the loss of functionality observed

dx.doi.org/10.1021/cs2001237 |*ACS Catal.* 2011, 1, 719–728

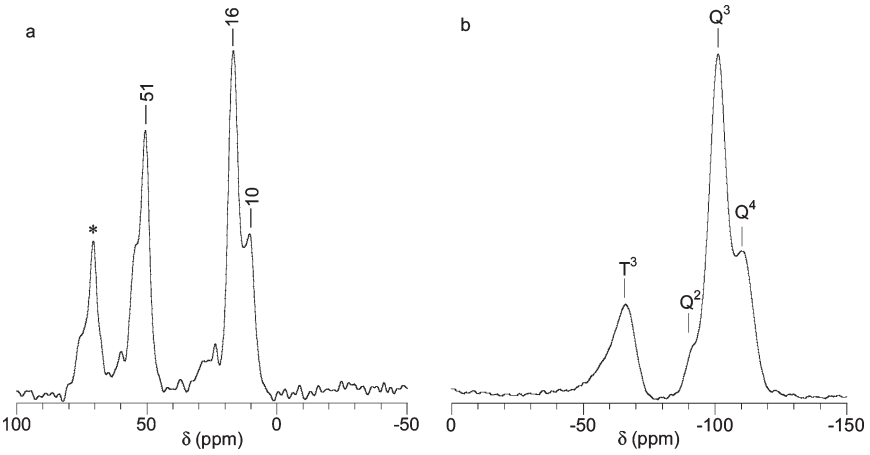

Figure 8. Solid-state NMR for SSA-SBA-15: (a) ^{13}C CP/MAS; and (b) ^{29}Si CP/MAS spectra. Spinning rate 10 kHz. * indicates surfactant signals.

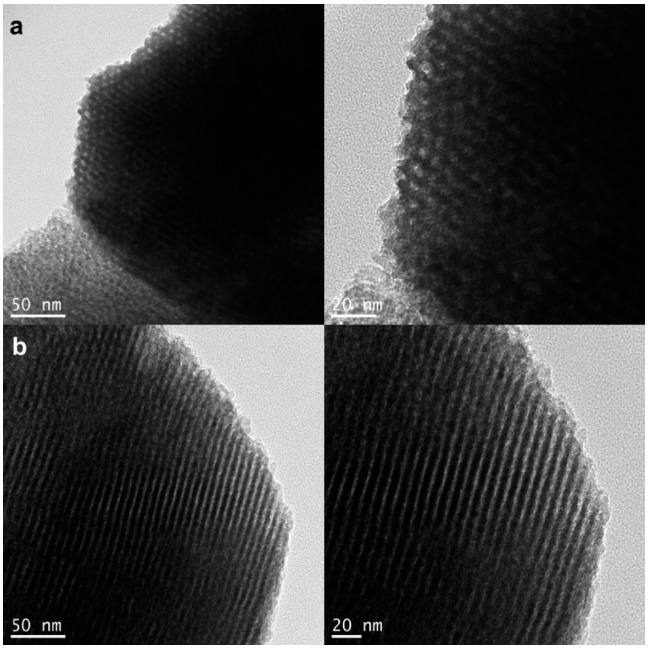

Figure 9. TEM images of SSA-SBA-15, showing (a) the hexagonally ordered mesopores; and (b) the parallel pore channels.

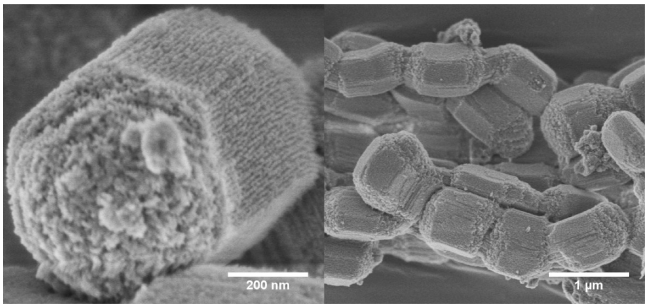

Figure 10. SEM images of SSA-SBA-15.

in our previous, multistep synthesis of bifunctionally modified SBA-15,[24] we prepared a new organosilane, TESAS. With some adjustments to the synthesis procedure, it was successfully incorporated into SBA-15 while maintaining mesopore ordering. We also synthesized a derivative in which the thioether was oxidized in situ to the corresponding sulfone (SSA-SBA-15).

The extent of incorporation of an organosilane into a silica matrix by co-condensation with a tetra(alkoxy)silane depends on the relative hydrolysis rates of the various silanes, as well as their interactions with the templating surfactant.[49] The organosilane may not be incorporated quantitatively, or may be partially inaccessible. For example, based on acidity measurements, less than 80% of the nominal MPTMS content was successfully oxidized in the synthesis of propylsulfonic acid-functionalized-SBA-15.[11] Either MPTMS was not fully incorporated, or the oxidant (H_2O_2) was unable to reach it. These problems arise from the tendency of organosilanes to disrupt the cooperative assembly of ordered silica, as well as their preference to undergo homocondensation.[49] Homocondensed organosilanes are not incorporated into the silica, and are removed during subsequent filtration. Increasing the organosilane to tetra(alkoxy)silane ratio may be desired to obtain higher functional group loadings; however, the mesopore ordering usually suffers.

The synthesis conditions required to obtain an ordered mesoporous silica depend on the functional group to be incorporated. TESAS is more complex than other silanes that have been inserted into ordered silicas, and the standard methods used to synthesize SBA-15 by co-condensation did not produce the desired structure, nor was the incorporation of the organosilane uniform. In hydrothermal synthesis, the organosilane is typically introduced into the reaction mixture 45 min after the addition of TEOS.[11,50] During the intervening time, TEOS hydrolyzes and begins to condense around the cylindrical micelles, then cross-condenses to form the hexagonal pore network.[49,51,52] Organosilanes added at this stage are believed to be less likely to disrupt the ordered framework or to undergo homocondensation, resulting in silicas with higher functional group loadings. However, the use of this synthesis procedure with TESAS resulted in only a silica gel and unordered TESAS-silica powder. When TESAS and TEOS were added to the synthesis mixture simultaneously, a gel was the exclusive product. The appearance of unordered silica powders and/or gels suggests that TESAS thoroughly disrupts the co-operative assembly process. In an attempt to mitigate this interference, TMOS was utilized instead of TEOS as the silica source. The faster condensation rate of TMOS led to the formation of ordered SBA-15, but resulted in a low content of accessible TESAS (0.15 mmol g^{-1}).

dx.doi.org/10.1021/cs2001237 |*ACS Catal.* 2011, 1, 719–728

Table 3. Rates of HMF Production over Various Solid Acid Catalysts[a]

catalyst	rate,[b] μmol HMF min^{-1}	catalyst loading, μmol H^+	TOF, min^{-1}
TESAS-SBA-15	7.2	22.5	0.32
Phosphonics Si-SPhSA	11	37.5	0.30
SSA-SBA-15	8.3	39.5	0.21
pSO_3H-SBA-15	10	55.0	0.19
Amberlyst 70	20	128	0.16

[a] Each reaction was carried out at 130 °C with 50 mg of catalyst, 1.5 g of aqueous phase (30 wt % fructose), and 3.0 g of organic phase (7:3 MIBK:2-butanol). [b] Rates are approximately constant (pseudo-zero-order) up to about 70% conversion. The data used to obtain the rates are shown in Supporting Information, Figure S8.

Table 4. Selectivity in the Dehydration of Fructose to HMF over Various Solid Acid Catalysts[a]

catalyst	mass,[b] mg	reaction time, min	conversion, %	selectivity, %
TESAS-SBA-15	142	141	84	71
Phosphonics Si-SPhSA	85.0	115	79	67
pSO_3H-SBA-15	58.0	140	79	66
SSA-SBA-15	82.0	140	81	65
Amberlyst 70	25.0	225	85	60

[a] Reactions were carried out at 130 °C with 1.5 g of aqueous phase (30 wt % fructose), and 3.0 g of organic phase (7:3 MIBK:2-butanol). [b] In each run, the catalyst loading corresponds to 64 μmol of acid (i.e., substrate/catalyst = 39).

To accommodate the complex organosilane and obtain a highly functionalized MOS, optimization of the synthesis procedure was necessary. Two modifications to the standard synthesis of organofunctionalized SBA-15 were made: first, NaCl was added to the reaction mixture after TEOS hydrolysis was initiated, and second, TESAS was added slowly over several hours. Simple inorganic salts have been suggested to improve the ordering of SBA-15 by promoting attractive interactions between the surfactant and the silane, and by improving the uniformity of the templating micelles.[52] Incremental organosilane addition was implemented to prevent TESAS homocondensation and to minimize disruptive TESAS-template interactions. These modifications yielded SBA-15 type silica with a high loading and uniform distribution of accessible TESAS. Furthermore, the addition of H_2O_2 to the TESAS-SBA-15 synthesis mixture led directly to similarly high-quality SSA-SBA-15.

Since TEOS encapsulates and cross-condenses around the surfactant micelles, we expected that delaying the addition of the organosilane to the synthesis mixture would yield fewer pore-oriented functional sites. For TESAS-SBA-15, elemental analysis showed that all of the organosilane was successfully incorporated into the silica framework (1.25 mmol g^{-1}), but only a third (0.45 mmol g^{-1}) of the sites were accessible by titration. This result suggests that the majority of TESAS sites resides within the pore walls. All subsequent TESAS-SBA-15 batches had similar, low accessible acid contents of about 0.40 mmol/g, as assessed by potentiometric titration. However, the functional site distribution also appears to depend on the chemical properties of the organosilane. When SSA-SBA-15 was synthesized by adding H_2O_2 after the complete addition of TESAS and 5 h after the addition of TEOS, essentially all of the incorporated SSA sites were accessible (0.80 mmol g^{-1}). It is possible that the silica framework is still capable of rearranging during the early stages of its synthesis. Thioether oxidation reduces the hydrophobicity of the alkyl chain, improving the interaction between SSA and the hydrophilic corona of the templating micelle, and providing a driving force for this rearrangement.

Particle Structure. Control over SBA-15 particle size and morphology can be exerted by the timed addition of an inorganic salt to the synthesis mixture. For example, Linton et al. recently obtained hexagonal platelets by introducing 0.1 M NaCl at 15 min after the addition of TMOS to an acidic solution (1.6 M HCl) containing 2.5 wt % Pluronic P104 at 50 °C.[42] There are few reports on controlling the particle morphology of organofunctionalized SBA-15 silicas synthesized by co-condensation, for the reasons discussed above.[34,53] To our knowledge, there are as yet no reports of SBA-type organosilicas with hexagonal particle morphology synthesized in this manner.

Using a different surfactant (Pluronic P123), a different silica source (TEOS), and a lower reaction temperature than Linton et al., and adding the NaCl later (30 min after initiation of hydrolysis), we obtained hexagonally shaped particles of both TESAS-SBA-15 and SSA-SBA-15. Nearly equilateral hexagonal particles were observed ranging from 0.5 to 1 μm in width and about 1 μm in thickness, with minimal defects, Figure 7. For SSA-SBA-15, addition of H_2O_2 during synthesis altered the particle morphology slightly, Figure 10. Elongated, thicker, but still well-proportioned hexagonal particles were observed. For both TESAS-SBA-15 and SSA-SBA-15, hexagonal particle growth in the presence of the organosilane appears to be promoted by the slow addition of the silane. In contrast, only cylindrical particles of pSO_3H-SBA-15 were observed by SEM, Supporting Information, Figure S3. However, in this case, the organosilane (MPTMS) was added somewhat more rapidly, over the course of one rather than four hours.

Reactivity toward Fructose. Three benchmark catalysts containing sulfonic acid groups were selected for comparison in the dehydration of fructose to HMF: an arylsulfonic acid resin (Amberlyst 70), an arylsulfonic acid-functionalized nonordered silica (Phosphonics Si-SPhSA), and propylsulfonic acid-functionalized SBA-15. TESAS-SBA-15, SSA-SBA-15 and the two silica-based benchmark catalysts are all efficient fructose dehydration catalysts, showing similar activities and selectivities. Given the modest differences in rate and selectivity for TESAS-SBA-15 and SSA-SBA-15, oxidation of the thioether to the sulfone was not effective in promoting the reaction, although the presence of the thioether itself appears to have a positive effect. Thus TESAS-SBA-15 is somewhat more active and selective than pSO_3H-SBA-15. We suspect that increased pore hydrophobicity contributes to the effect. Interestingly, Phosphonics Si-SPhSA, which contains more acidic arylsulfonic acid groups, behaved very similarly to alkylsulfonic acid-containing TESAS-SBA-15. Amberlyst 70, which is significantly different from the other catalysts both in composition (polymer-based rather than silica-based) and acid site density (2.55 vs ≤1.1 mmol g^{-1}), showed the lowest TOF and selectivity.

Some expected byproducts[35] were observed: insoluble humins and levulinic acid. Difructose anhydrides (DFAs), an example of which is shown in Scheme 1, were also formed. DFAs form by

elimination of two molecules of water, with formation of two glycosidic bonds.[35,54,55] Products whose molecular weights suggest addition reactions of HMF with itself, and of HMF with 2-butanol, are likely ethers, as reported in the literature.[35,56,57] Finally, the formation of a compound with a molecular weight corresponding to the addition of HMF to MIBK could be an aldol condensation product, analogous to that seen in the reaction of HMF with acetone under basic conditions.[58]

CONCLUSIONS

Silica-supported alkylsulfonic acids are efficient and selective fructose dehydration catalysts under batch conditions. Morphological control in these co-condensed mesoporous silicas can be achieved through optimization of the timing and rate of salt and organosilane additions. Tuning the morphology and pore dimensions while ensuring robust attachment of the functional groups via co-condensation may be critical in catalytic and separations applications. In future work, it will be important to assess the importance of morphology on activity and hydrothermal stability.

ASSOCIATED CONTENT

Supporting Information. Additional synthetic details, characterization of pSO_3H-SBA-15 by N_2 adsorption/desorption, TEM, SEM, XPS, and solid-state CP-MAS NMR (^{13}C and ^{29}Si). Details of HMF rate measurements and LC/MS results are also included. This material is available free of charge via the Internet at http://pubs.acs.org.

AUTHOR INFORMATION

Corresponding Author

*E-mail: dumesic@engr.wisc.edu (J.A.D.), sscott@engineering.ucsb.edu (S.L.S.).

ACKNOWLEDGMENT

The authors thank Dr. Huang Kai and Dr. Jin-Ping Zhang of the Suzhou Institute of Nano-Tech and Nano-Bionics for their assistance in collecting the SEM images. This work was supported by the NSF under the auspices of the Center for Enabling New Technologies through Catalysis (CENTC). A.J.C. acknowledges the PIRE-ECCI (NSF Grant OISE-0530268) for a fellowship. Portions of this work made use of facilities of the Materials Research Laboratory, supported by the MRSEC Program of the National Science Foundation under award No. DMR05-20415.

REFERENCES

(1) Yiu, H. H. P.; Botting, C. H.; Botting, N. P.; Wright, P. A. *Phys. Chem. Chem. Phys.* **2001**, *3*, 2983–2985.
(2) Ciesla, U.; Schüth, F. *Microporous Mesoporous Mater.* **1999**, *27*, 131–149.
(3) Davis, M. E. *Nature* **2002**, *417*, 813–821.
(4) Lei, B.; Li, B.; Zhang, H.; Zhang, L.; Li, W. *J. Phys. Chem. C* **2007**, *111*, 11291–11301.
(5) Mellaerts, R.; Aerts, C. A.; Humbeeck, J. V.; Augustijns, P.; den Mooter, G. V.; Martens, J. A. *Chem. Commun.* **2007**, 1375–1377.
(6) Trewyn, B. G.; Giri, S.; Slowing, I. I.; Lin, V. S. Y. *Chem. Commun.* **2007**, 3236–3245.
(7) Corma, A. *Chem. Rev.* **1997**, *97*, 2373–2420.
(8) Zhao, D.; Feng, J.; Huo, Q.; Melosh, N.; Fredrickson, G. H.; Chmelka, B. F.; Stucky, G. D. *Science* **1998**, *279*, 548–552.
(9) Zhao, D.; Huo, Q.; Feng, J.; Chmelka, B. F.; Stucky, G. D. *J. Am. Chem. Soc.* **1998**, *120*, 6024–6036.
(10) Huh, S.; Wiench, J. W.; Yoo, J.-C.; Pruski, M.; Lin, V. S. Y. *Chem. Mater.* **2003**, *15*, 4247–4256.
(11) Margolese, D.; Melero, J. A.; Christiansen, S. C.; Chmelka, B. F.; Stucky, G. D. *Chem. Mater.* **2000**, *12*, 2448–2459.
(12) Trewyn, B. G.; Slowing, I. I.; Giri, S.; Chen, H.-T.; Lin, V. S. Y. *Acc. Chem. Res.* **2007**, *40*, 846–853.
(13) Vansant, E. F.; Van Der Voort, P.; Vrancken, K. C. *Stud. Surf. Sci. Catal.* **1995**, *93*, 149–192.
(14) Burkett, S. L.; Sims, S. D.; Mann, S. *Chem. Commun.* **1996**, 1367–1368.
(15) Wirnsberger, G.; Scott, B. J.; Stucky, G. D. *Chem. Commun.* **2001**, 119–120.
(16) Baleizão, C. G., B.; Das, D.; Álvaro, M.; Garcia, H.; Corma, A. *J. Catal.* **2004**, *223*, 106–113.
(17) Chen, H.-T.; Huh, S.; Wiench, J. W.; Pruski, M.; Lin, V. S. Y. *J. Am. Chem. Soc.* **2005**, *127*, 13305–13311.
(18) Hoffmann, F.; Fröba, M. In *The Supramolecular Chemistry of Organic-Inorganic Hybrid Materials*; Rurack, K., Martinez-Manez, R., Eds.; Wiley: Hoboken, NJ, 2010; pp 37−111.
(19) Slowing, I. I.; Vivero-Escoto, J. L.; Trewyn, B. G.; Lin, V. S. Y. *J. Mater. Chem.* **2010**, *20*, 7924–7937.
(20) Brunel, D. *Microporous Mesoporous Mater.* **1999**, *27*, 329–344.
(21) Clark, J. H.; Macquarrie, D. J. *Chem. Commun.* **1998**, 853–860.
(22) Descalzo, A. B.; Marcos, M. D.; Martinez-Manez, R.; Soto, J.; Beltran, D.; Amoros, P. *J. Mater. Chem.* **2005**, *15*, 2721–2731.
(23) Acosta, E.; Carr, C.; Simanek, E.; Shantz, D. *Adv. Mater.* **2004**, *16*, 985–989.
(24) Crisci, A. J.; Tucker, M. H.; Dumesic, J. A.; Scott, S. L. *Top. Catal.* **2010**, *53*, 1185–1192.
(25) Dais, P.; Perlin, A. S. *Carbohydr. Res.* **1985**, *136*, 215.
(26) Dais, P.; Perlin, A. S. *Carbohydr. Res.* **1987**, *169*, 159.
(27) Roman-Leshkov, Y.; Chheda, J. N.; Dumesic, J. A. *Science* **2006**, *312*, 1933–1937.
(28) Zhao, D.; Sun, J.; Li, Q.; Stucky, G. D. *Chem. Mater.* **2000**, *12*, 275–279.
(29) Lee, H. I.; Kim, J. H.; Stucky, G. D.; Shi, Y.; Pak, C.; Kim, J. M. *J. Mater. Chem.* **2010**, *20*, 8483–8487.
(30) Taguchi, A.; Schüth, F. *Microporous Mesoporous Mater.* **2005**, *77*, 1–45.
(31) Schmidt-Winkel, P.; Yang, P.; Margolese, D. I.; Chmelka, B. F.; Stucky, G. D. *Adv. Mater.* **1999**, *11*, 303–307.
(32) Konya, Z.; Zhu, J.; Szegedi, A.; Kiricsi, I.; Alivisatos, P.; Somorjai, G. A. *Chem. Commun.* **2003**, 314–315.
(33) Zhang, H.; Sun, J.; Ma, D.; Bao, X.; Klein-Hoffmann, A.; Weinberg, G.; Su, D.; Schlögl, R. *J. Am. Chem. Soc.* **2004**, *126*, 7440–7441.
(34) Chen, S.-Y.; Tang, C.-Y.; Chuang, W.-T.; Lee, J.-J.; Tsai, Y.-L.; Chan, J. C. C.; Lin, C.-Y.; Liu, Y.-C.; Cheng, S. *Chem. Mater.* **2008**, *20*, 3906–3916.
(35) Kuster, B. F. M. *Starch/Stärke* **1990**, *42*, 314–321.
(36) Roman-Leshkov, Y.; Barrett, C. J.; Liu, Z. Y.; Dumesic, J. A. *Nature* **2007**, *447*, 982–985.
(37) Lansalot-Matras, C.; Moreau, C. *Catal. Commun.* **2003**, *4*, 517–520.
(38) Zhao, H. B.; Holladay, J. E.; Brown, H.; Zhang, Z. C. *Science* **2007**, *316*, 1597–1600.
(39) Gran, G. *Anal. Chim. Acta* **1988**, *206*, 111–123.
(40) Cinlar, B.; Shanks, B. H. *Appl. Catal., A* **2011**, *396*, 76–84.
(41) Lesaint, C.; Lebeau, B.; Marichal, C.; Patarin, J. *Microporous Mesoporous Mater.* **2005**, *83*, 76–84.
(42) Linton, P.; Wennerstrom, H.; Alfredsson, V. *Phys. Chem. Chem. Phys.* **2010**, *12*, 3852–3858.

(43) Wagner, C. D.; Muilenberg, G. E. *Handbook of X-ray Photoelectron Spectroscopy*; Perkin-Elmer Corp., Physical Electronics Division: Eden Prairie, MN, 1979.
(44) Holm, R. In *Analysis of Organic and Biological Surfaces*; Echlin, P., Ed.; Wiley: New York, 1984; pp 37−72.
(45) Shen, J. G. C.; Herman, R. G.; Klier, K. *J. Phys. Chem. B* **2002**, *106*, 9975–9978.
(46) Mori, Y.; Pinnavaia, T. J. *Chem. Mater.* **2001**, *13*, 2173–2178.
(47) Flodström, K.; Teixeira, C. V.; Amenitsch, H.; Alfredsson, V.; Lindén, M. *Langmuir* **2004**, *20*, 4885–4891.
(48) Robinson, D. J.; Davies, L.; McGuire, N.; Lee, D. F.; McMorn, P.; Willock, J.; Watson, G. W.; Page, P. C. B.; Bethell, D.; Hutchings, J. *Phys. Chem. Chem. Phys.* **2000**, *2*, 1523–1529.
(49) Hoffmann, F.; Cornelius, M.; Morell, J.; Fröba, M. *Angew. Chem., Int. Ed.* **2006**, *45*, 3216–3251.
(50) Mbaraka, I. K.; Shanks, B. H. *J. Catal.* **2005**, *229*, 365.
(51) Fan, J.; Boettcher, S. W.; Tsung, C.-K.; Shi, Q.; Schierhorn, M.; Stucky, G. D. *Chem. Mater.* **2008**, *20*, 909–921.
(52) Wan, Y.; Zhao, D. *Chem. Rev.* **2007**, *107*, 2821–2860.
(53) He, Q.; Shi, J.; Cui, X.; Zhao, J.; Chen, Y.; Zhou, J. *J. Mater. Chem.* **2009**, *19*, 3395–3403.
(54) van Dam, H. E.; Kieboom, A. P. G.; van Bekkum, H. *Starch/Stärke* **1986**, *38*, 95–101.
(55) Gattuso, G.; Nepogodiev, S. A.; Stoddart, J. F. *Chem. Rev.* **1998**, *98*, 1919–1958.
(56) Bicker, M.; Kaiser, D.; Ott, L.; Vogel, H. *J. Supercrit. Fluids* **2005**, *36*, 118–126.
(57) Casanova, O.; Iborra, S.; Corma, A. *J. Catal.* **2010**, *275*, 236–242.
(58) Chheda, J. N.; Dumesic, J. A. *Catal. Today* **2007**, *123*, 59–70.